BEHIND ARMOR DEBRIS DISTRIBUTION AFTER KE ROD PERFORATION OF RHA PLATES FOR DISTINCT OVERMATCH CONDITIONS

Karl Weber

Fraunhofer Ernst-Mach-Institut (EMI), Eckerstrasse 4, 79104 Freiburg, Germany;
Phone: +49(0)761/2714-323, Fax: +49(0)761-1323, email: weber@emi.fhg.de

Experiments have been performed with L/D = 6 WSA rods against RHA targets with thicknesses of T = 3-125mm due to overmatches of OM = 0.98-0.19 at normal and oblique impacts at v_P = 1700m/s. Amount, mass and lateral spread of the fragments increase with increasing target obliquity and RHA thickness, achieve a maximum for T = 70mm and decrease again for T > 70mm. Application of PE liners diminish amount and emission angle of the fragments.

INTRODUCTION

Armored vehicles have to be protected against a wide range of threats such as mines, fragments, KE rods and shaped charge jets. When a KE rod perforates a target the resulting debris is a major component of the lethal effects behind the armor. In this paper the data of recently performed experiments on the debris distribution behind RHA plates for distinct overmatch conditions at normal and oblique impacts are presented.

TEST SET-UPS AND TEST MATRIX

The experiments have been performed with a tungsten sinter alloy (WSA) rod with a mass of m_P = 670g, a diameter of D = 20mm and a length-to-diameter ratio of L/D = 6 at an impact velocity of v_P = 1700m/s. The KE rods were shot against single-plate RHA targets with a Vickers hardness number of VHN = 330-351 at normal (ϑ = Nato 0°) and oblique impact (ϑ = Nato 60°) using the test set-ups of Figures 1 and 2.

In case of the Nato 0° targets the plate thickness ranged between T = 3mm and T = 125mm. For investigation of the liner influence on the fragment distribution behind the 70mm RHA plates, homogeneous polyethylene (PE) liners with thicknesses of T_L = 20, 30 and 50mm, a material density of ρ_L = 0.95g/cm^3 and a shore hardness number of SHN = 62 were bonded on the 70mm RHA plate by means of a polyurethane-based adhesive. Pitch and yaw angles before impact were controlled with the 150 kV flash

X-rays X_1 and X_2. Length and velocity of the residual rod as well as debris cloud formation have been observed with the flash X-rays X_3-X_5. For evaluation of the fragment parameters such as material, size, shape, amount, angular and mass distributions a soft recovery stack consisting of 65 sheets of 10mm thick soft fiber plates with lateral dimensions of 120 x 120cm has been arranged 800mm behind the target assembly. For each parameter two experiments have been performed, for the thinner plates of T = 3-25mm only one test was carried out (16 tests total at normal impact).

The experiments at ϑ = Nato 60° were carried out against RHA plates with T = 35, 45 and 62.5mm corresponding to line-of-sights of LOS = 70, 90 and 125mm, respectively. The PE liners with thicknesses of T_L = 20, 30 and 50mm were attached to the 70mm RHA. The soft recovery stack has been arranged 340mm behind the target assembly at $\vartheta/2$ = Nato 30°. At oblique impact, 12 tests total were carried out.

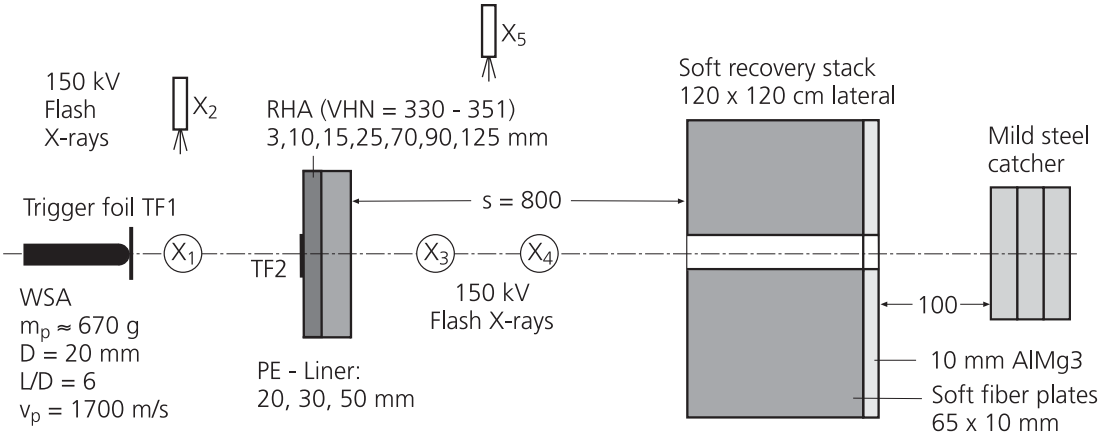

Figure 1. Test set-up of single-plate targets at normal impact (ϑ = Nato 0°)

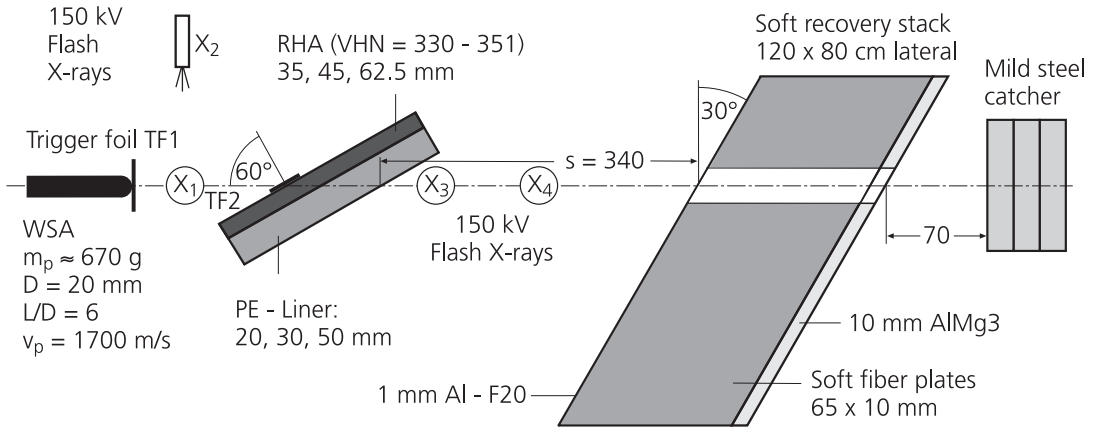

Figure 2. Test set-up of single-plate targets at oblique impact (ϑ = Nato 60°)

INFLUENCES ON RESIDUAL ROD AND DEBRIS CLOUD FORMATION

In the following, the influences of target obliquity, RHA plate and PE liner thicknesses on residual performance of the KE rod after perforation of the target as well as fragment distribution behind the target are considered.

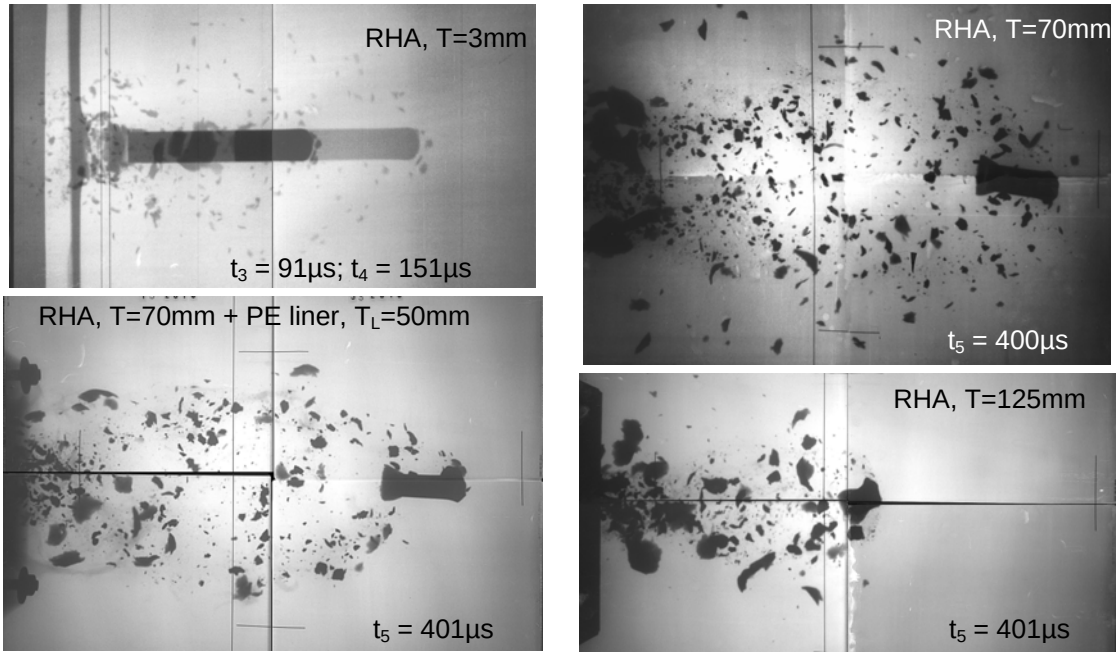

Figure 3. Influences of RHA plate thickness (T = 3, 70 and 125mm) and PE liner (T_L = 50mm) on debris cloud formation at normal impact (v_P = 1700m/s)

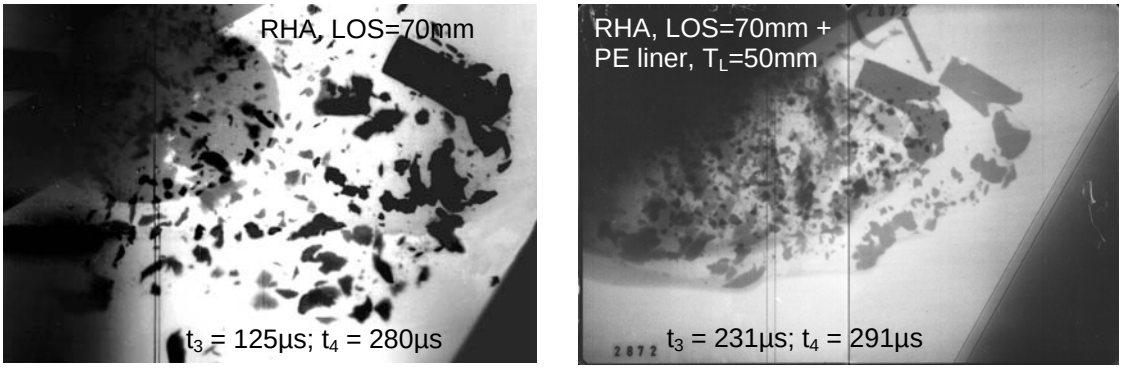

Figure 4. Debris cloud formation behind a RHA single-plate target with LOS = 70mm and focusing effect by a PE liner of T_L = 50mm at oblique impact (v_P = 1700m/s)

In the flash X-ray photographs of Figure 3 residual rod and debris cloud are shown behind RHA plates with T = 3, 70 and 125mm at normal impact. In case of thin RHA plates (T = 3mm) the KE rod is only slightly reduced in length and velocity and mostly small fragments are distributed around the residual rod.

With increasing T the resistance of the target against penetration increases resulting in further residual length L_R and velocity v_R reductions. At T = 70mm the rod length is already reduced to $L_R/L \approx 0.5$. An expanding cloud with a maximum amount of fragments is observed. At distinctly larger plate thickness of T = 125mm the residual rod length is diminished to $L_R \approx 0.2 \cdot L$. The number of fragments has decreased but the fragments are larger.

In Figure 4 flash X-ray photographs of the debris distribution for RHA targets with LOS = 70mm are presented. In comparison to the corresponding previous experiments at normal impact the flash X-ray double exposures are taken at earlier times. At oblique impact the residual rod is rotated and partly broken during perforation of the target. The debris cloud expands asymmetrically in the plane of symmetry, whereas the fragment size distribution is comparable to normal impact.

Application of a liner on the rear side of a target diminishes amount and lateral spread of the secondary fragments as a result of retardation and focusing effects [1, 2], demonstrated in Figures 3 and 4 for the 50mm thick PE liner attached on the rear side of a RHA target with LOS = 70mm at normal and oblique impacts, respectively.

Residual Rod Length and Velocity

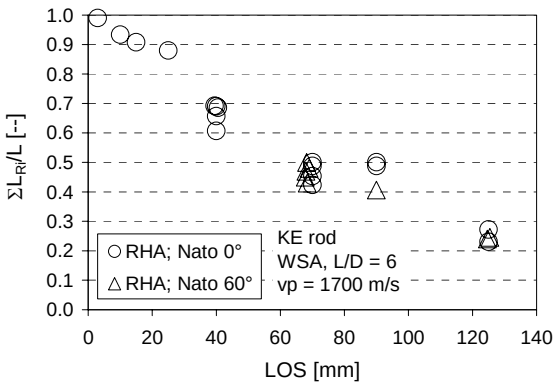

Figure 5. Residual length $\Sigma L_R/L$ vs. line-of-sight LOS at normal and oblique impacts

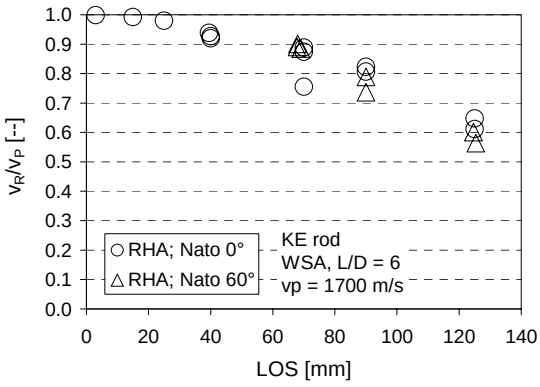

Figure 6. Residual velocity v_R/v_P vs. line-of-sight LOS at normal and oblique impacts

From the flash X-ray photographs residual length and velocity of the L/D = 6 rod after perforation of the single-plate targets with LOS = 3-125mm corresponding to an overmatch of OM = 0.98-0.19 have been determined. The overmatch, defined by the

relation OM = (p_∞ - LOS)/p_∞, is a measure for the residual energy of a KE rod after perforation of a target. For the L/D = 6 KE rod an average penetration depth of $\bar{p}_\infty$ = 154.9mm has been found in semi-infinite RHA at v_P = 1700m/s. The thinner the plate, the higher the OM-value and the higher the energy of the residual rod behind the target.

The normalized residual length $\Sigma L_R/L$ and residual velocity v_R/v_P, dependent on LOS, for the RHA targets without liner at normal and oblique impacts are depicted in Figures 5 and 6, respectively. $\Sigma L_R/L$ and v_R/v_P strongly decrease with increasing LOS. At identical LOS the data points of the targets at Nato 60° are slightly below the corresponding values at Nato 0° due to additional bending and breaking effects as well as deflection and rotation of the rod during the perforation process. Influence of liner plate thickness on L_R and v_R was within the data scatter and can be neglected.

Projectile and Target Fragment Distribution in Soft Recovery Stack

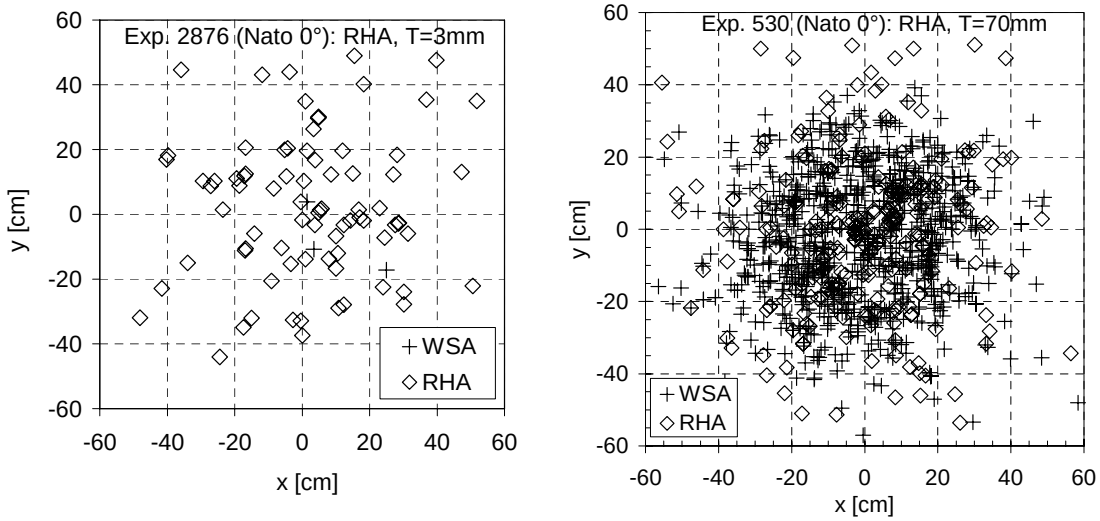

Figure 7. Projectile and target fragment distribution in soft recovery stack dependent on RHA thickness at normal impact; left: 3mm RHA; right: 70mm RHA [3]

By means of soft recovery stack evaluations, detailed data collection has been separately performed for projectile and target fragments. Scatter diagrams of typical fragment distributions are shown in Figure 7 for 3mm and 70mm RHA at Nato 0°.

In case of the 3mm RHA, the target fragments are more or less homogeneously spread over the entire area of the soft catcher. Only a few number of tungsten fragments has been found. For the 70mm RHA target, a large amount of WSA and RHA fragments has been generated due to the higher penetration resistance of the target and the larger crater volume.

Maximum Amount and Mass of Small-Size and Ring Fragments

In case of normal impact, crater volume in the target plate and volume of eroded penetrator material increases with increasing plate thickness resulting in an increase of amount and mass of projectile and target fragments up to a critical target thickness T_{crit} ("saturation thickness"). For $T > T_{crit}$, amount and mass of fractured rod and target materials are diminished again due to the decreasing degree of fragmentation and crater cross section for increasing T.

At constant line-of-sight (LOS), increasing target obliquity leads to a diminishment of target plate thickness accompanied by a growing crater volume in the target plate, demonstrated in the diagrams of Figures 8 and 9 for the target obliquity angles of Nato 0° and Nato 60°, respectively.

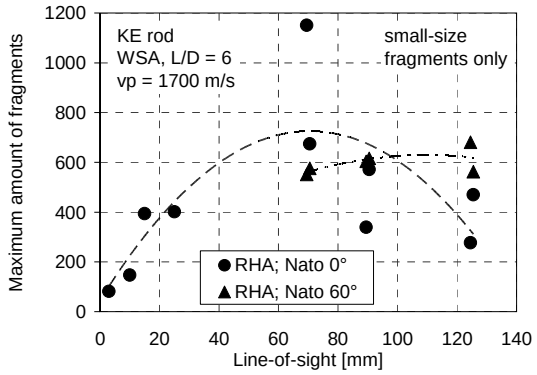

Figure 8. Maximum amount of fragments versus line-of-sight at normal and oblique impacts

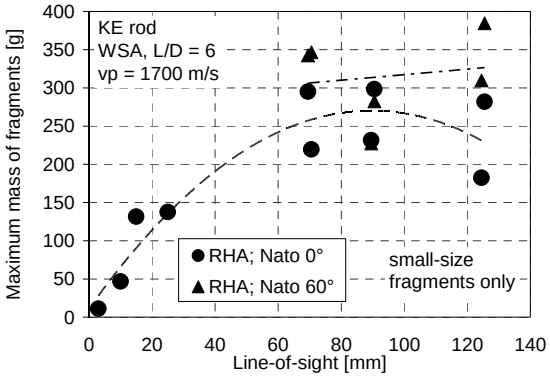

Figure 9. Maximum fragment mass versus line-of-sight at normal and oblique impacts

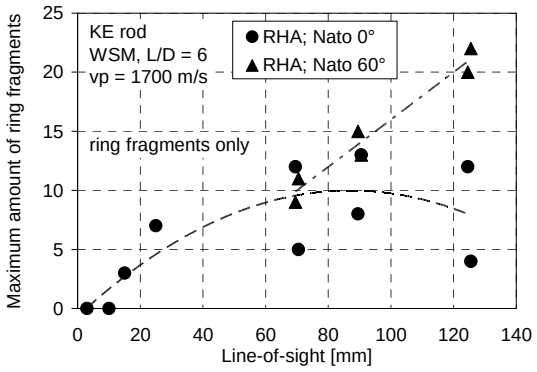

Figure 10. Maximum amount of ring fragments versus line-of-sight at normal and oblique impacts

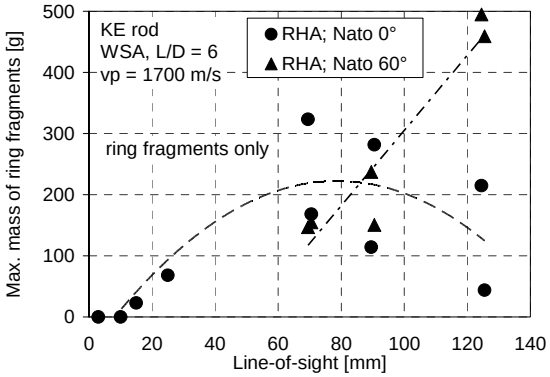

Figure 11. Maximum mass of ring fragments versus line-of-sight at normal and oblique impacts

Whereas, the results for the small-size fragments with masses $m_{SF} \leq 5g$ are shown in Figures 8-9, the outcomes for the ring-fragments with masses $m_{RF} > 5g$ are depicted separately in Figures 10-11. Comparison of the diagrams in Figures 8-9 and Figures 10-11 give evidence of a similar curve progression for small-size and ring fragments, respectively. As shown in the diagrams, the maximum mass of small-size and ring fragments is comparable. However, the maximum amount of small-size fragments is distinctly higher than the total number of the ring fragments. The largest ring fragments can achieve masses of several tens up to more than one hundred grams.

Maximum Emission Angle

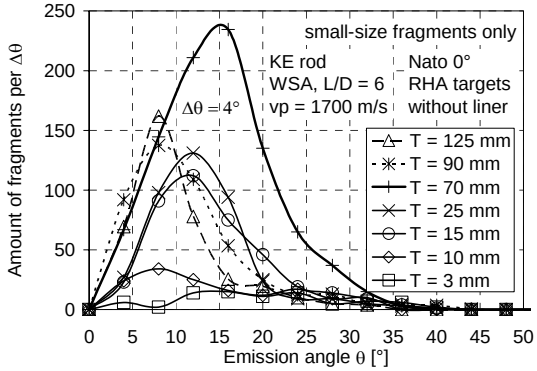

Figure 12. Amount of fragments per Δθ vs. θ for RHA with T = 3-125mm at normal impact

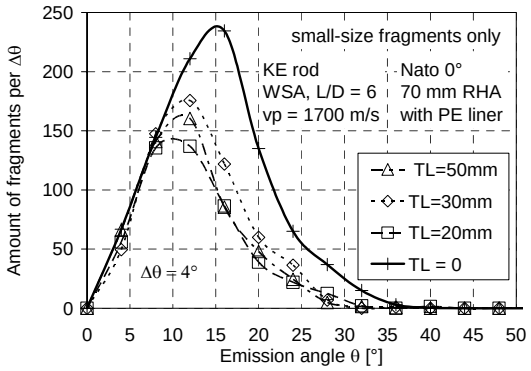

Figure 13. Amount of fragments per Δθ vs. θ for 70mm RHA + PE liners (T_L=0-50mm) at Nato 0°

At normal impact, maximum emission angle θ_{max} and amount of fragments ΔN per angle interval $\Delta\theta$ ($\Delta\theta = 4°$) increase with increasing plate thickness as long as $T < T_{crit} = 70mm$, shown in Figure 12 for the small-size WSA and RHA fragments. For $T > T_{crit}$, θ_{max} and $(\Delta N/\Delta\theta)_{max}$ decrease again with increasing T due to reduced crater cross sections at lower overmatch values. Application of PE liner leads to a diminishment of the maximum amount of fragments per angle interval $(\Delta N/\Delta\theta)_{max}$ and the maximum emission angle θ_{max} with increasing liner plate thickness T_L. In addition, for thicker PE liners $(\Delta N/\Delta\theta)_{max}$ is shifted to smaller emission angles (Figure 13).

The lateral fragment spread increases with increasing target obliquity, demonstrated in Figures 14 and 15 at Nato 0° and Nato 60°. At Nato 60°, the maximum emission angle θ_{max} is well above the corresponding θ_{max}-values at Nato 0°. θ_{max} decreases with increasing RHA plate (LOS) and PE liner thicknesses. Excluding "outlier", in Figures 14 and 15 the maximum emission angles for 100 % and 95 % of the fragments are compared. In the diagrams, only small-size projectile (WSA) and target (RHA) fragments are shown. Consideration of 95% of the fragments leads to a

reduction of the maximum emission angle, especially at oblique impact, but the influences of line-of-sight and liner thickness are qualitatively the same as for Nato 0°.

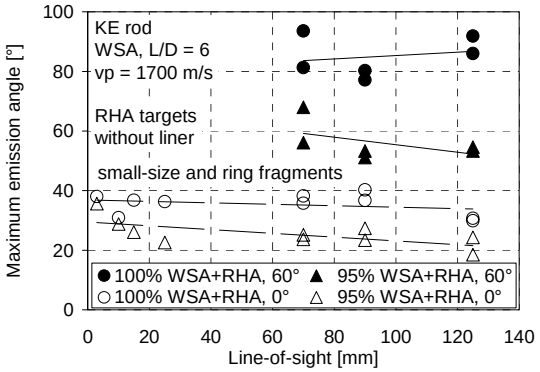

Figure 14. Maximum emission angle versus line-of-sight at normal and oblique impacts

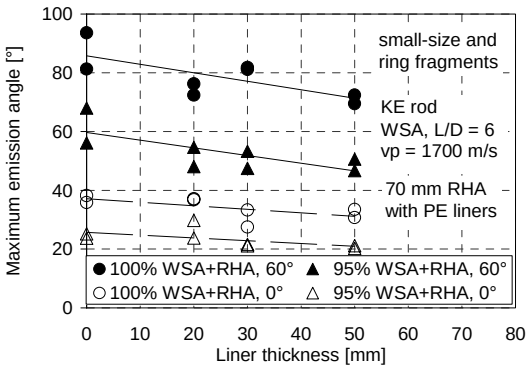

Figure 15. Maximum emission angle versus PE liner thickness at normal and oblique impacts

CONCLUSIONS

Experiments have been performed with L/D = 6 WSA rods against RHA targets with line-of-sights LOS = 3-125mm corresponding to overmatches of OM = 0.98-0.19 at normal and oblique impacts at an impact velocity of v_P = 1700m/s.

At normal impact, amount, mass and emission angle of the fragments increase with increasing target thickness T, achieve a maximum at $T = T_{crit}$ = 70mm ("saturation thickness") and decrease again for $T > T_{crit}$. The corresponding values at oblique impact are well above the data found at normal impact. The secondary fragment effects can be reduced by application of PE liners. Amount and lateral spread of the projectile and target fragments decrease with increasing liner thickness.

REFERENCES

[1] S. Lampert and R. Jeanquartier, Threat dependent protection efficacy of metal / liner compositions, *18th International Symposium on Ballistics*, San Antonio, TX, November 15-19, 1999

[2] W. Riedel, K. Weber, M. Wicklein, K. Thoma, and J. Färber, Reduction of fragment effects behind layered armour – experimental and numerical analysis, *21st International Symposium on Ballistics*, Adelaide, Australia, April 19-23, 2004

[3] K. Weber, K. Kleinschnitger, T. Behner, and V. Hohler, Influence of liners on the debris cloud expansion behind single-plate targets perforated by rod projectiles, *19th International Symposium on Ballistics*, Interlaken, Switzerland, May 7-11, 2001